Sensors and Materials, Vol. 38, No. 8 (2026) 4873–4884
MYU Tokyo

S & M 4599

Image-based Suspended Sediment Visualization and Diffusion Analysis Using Unmanned Aerial Vehicle

Hyung-Suk Kim,[1] Gyu-Seok Han,[1] Jae-Seon Yoon,[2] Woochul Kang,[3] and Seung-Bae Choi[1*]

[1]Department of Civil Engineering, Kunsan National University, South Korea
[2]Rural Research Institute, Korea Rural Community Corporation, South Korea
[3]Department of Smart Infrastructure Engineering, Kongju National University, South Korea

(Received November 24, 2025; accepted August 12, 2026)

Keywords: suspended sediment concentration, spatiotemporal mapping, sediment plume tracking

Anthropogenic activities such as urban development, waterfront expansion, and large-scale land reclamation increasingly disrupt sediment dynamics in rivers, estuaries, and coastal zones. These disturbances elevate suspended sediment concentration (*SSC*), degrading water quality by reducing light penetration, damaging benthic habitats, altering trophic interactions, and threatening biodiversity. Conventional *SSC* monitoring methods, such as manual sampling, fixed turbidity sensors, and satellite remote sensing, have limitations: manual sampling and sensors offer limited spatiotemporal data, whereas satellite imagery is costly, weather-dependent, and infrequent. To address these constraints, in this study, we propose a high-resolution *SSC* monitoring framework that integrates unmanned aerial vehicle (UAV)-acquired RGB imagery with *in situ* turbidity measurements. UAV images were processed via photogrammetry, including orthomosaic generation and pixel-level radiometric analysis. Brightness values from the red spectral channel, highly sensitive to sediment reflectance, were extracted. A linear regression model correlating these pixel values with field-measured *SSC* achieved strong predictive performance ($R^2 = 0.84$). Field experiments at a riverine sediment source confirmed the system's ability to detect rapid *SSC* increases on minute-to-hour scales and to identify sediment plume boundaries with high spatial accuracy. While promising, further validation across broader sediment compositions and turbidity conditions is needed. Incorporating multispectral or hyperspectral sensors can enhance predictive accuracy and expand applicability. Overall, this framework bridges the gap between fixed sensors and satellites, providing a flexible, scalable, and cost-effective solution for *SSC* monitoring.

1. Introduction

In recent years, the number of large-scale aquatic environment development projects, such as dredging, land reclamation, and port construction, in rivers, estuaries, and coastal areas has been increasing. These activities lead to rapid changes in the concentration of suspended sediment (SS), which has emerged as a serious environmental concern.[(1,2)] An increase in SS concentration reduces light penetration in the water column, inhibiting photosynthesis of

*Corresponding author: e-mail: ace8978@kunsan.ac.kr
https://doi.org/10.18494/SAM6200

ISSN 0914-4935
https://myukk.org/

phytoplankton and potentially disrupting the food web.[3] Furthermore, the sedimentation process alters the benthic environment and reduces dissolved oxygen concentration, thereby decreasing the species diversity of benthic invertebrates and affecting the overall aquatic ecosystem.[4,5] Such ecological changes often lead to a decline in fishery resources. In South Korea, there have even been cases in which the government compensated fisheries for losses linked to port-construction activities.[6] Thus, variations in SS concentration can trigger not only ecological degradation but also social and economic conflicts.

Accurate monitoring of SS concentration and assessment of its spatiotemporal distribution are keys to resolving these issues. There are three traditional methods for measuring SS concentration. First, direct water sampling and filtration analysis using a vessel provides high accuracy but produces one time, point-based data, making it difficult to capture continuous or large-scale variability.[7,8] Second, *in situ* sensors such as optical backscatter sensors (OBS) or acoustic Doppler current profilers (ADCP) allow for continuous temporal observation at a fixed point but have a limited spatial range, requiring increased equipment and cost to monitor a wide area.[9] Third, satellite or aerial remote sensing is useful for observing the surface SS distribution over a large area, but its fixed acquisition period limits temporal resolution, and data collection is difficult under adverse weather conditions.[10] Moreover, medium- to low-resolution imagery has limitations in detecting changes in narrow water bodies or small-scale events.[11] Consequently, while existing monitoring technologies have their own advantages, point-based time-series observation and spatial mapping are performed separately, limiting the ability to quantitatively and spatially grasp the rapidly changing SS behavior. Therefore, a new monitoring system that effectively fuses real-time *in situ* data with spatial imagery information is needed to quickly respond to SS diffusion and accurately assess environmental impacts at construction sites.

The objective of this study is to develop a spatial suspended sediment concentration (*SSC*) monitoring system that overcomes the limitations and combines the advantages of existing methods. Specifically, it aims to integrate real-time buoy-based observation data with unmanned aerial vehicle (UAV)-based orthomosaic imagery and establish a correlation between pixel intensity values and measured *SSC*, thereby visualizing the surface *SSC* of the target water body as a quantitative 2D map.

2. Materials and Methods

The spatial *SSC* monitoring system proposed in this study consists of three main components: (1) a system buoy for real-time data acquisition, (2) a UAV for spatial image collection, and (3) an analysis workflow that fuses these two data sources to visualize the 2D distribution of suspended sediment.

2.1 Configuration of near real-time monitoring system

The overall concept of the system is shown in Fig. 1. Multiple system buoys continuously measure surface turbidity and location data and transmit this data to a user server in real time

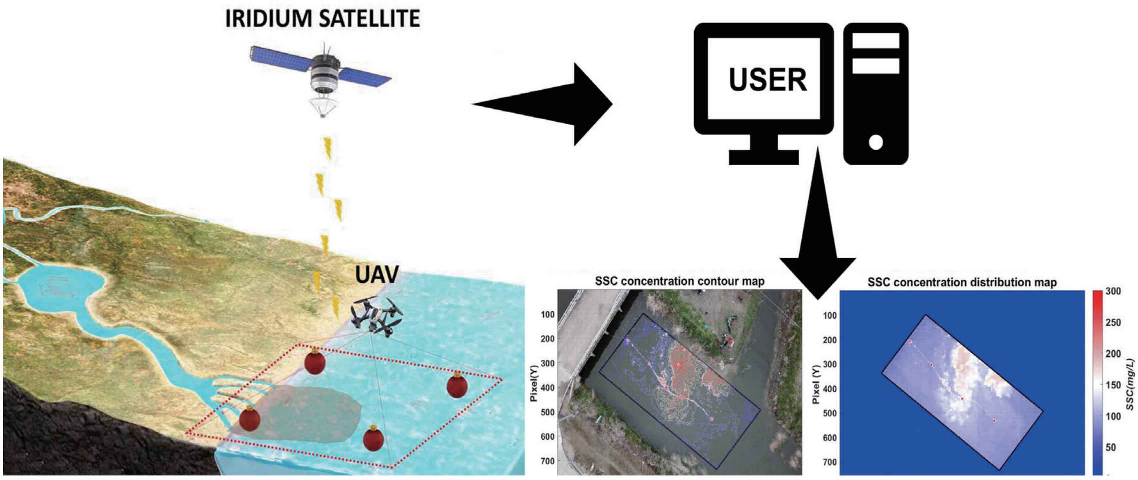

Fig. 1. (Color online) Conceptual configuration of the SSC monitoring system.

via satellite communication. Simultaneously, the UAV acquires a high-resolution orthoimage by conducting aerial photography of the same area. On the server, the buoy data and the pixel intensity values extracted from the image analysis are cross-calibrated to visualize the *SSC* distribution of the target water body as a 2D map.

2.2 System buoy for real-time observation

The integrated observation module collects and transmits field-measured data in real time, including *SSC*, water temperature, and location. *SSC* is measured using an OBS mounted on the buoy, and the data are simultaneously stored in internal memory and transmitted via an Iridium satellite communication module. The compact and waterproof buoy design ensures stable performance under field conditions. Table 1 summarizes the main specifications and components.

2.3 Acquisition of UAV orthoimages

A rotary-wing UAV (DJI Matrice 600 Pro) was employed to capture spatial imagery for monitoring suspended sediment distribution. The UAV provides stable hovering capabilities and is equipped with a 12.4-megapixel Zenmuse X3 gimbal camera to minimize vibrations during flight.[12] During the survey, the UAV hovered at an altitude of 50 m for approximately 10 min, achieving a ground sample distance (GSD) of about 3.76 cm/pixel.

The detailed specifications of the UAV used in this study are summarized in Table 2. These specifications ensured stable and precise image acquisition throughout the field survey.

Table 1
Specifications of the system board.

Component	Specification
System board	- Average power consumption: 1.56 mA - Processing system: 6–16 V - Memory: 256 kB program memory - Sleep mode current: down to 10 nA (typical) - Features: built-in RTC, satellite data transmission, adjustable acquisition interval
Buoy body & housing	- Spherical (~400 mm diameter) with urethane coating - Cylindrical waterproof housing accommodates sensor, control board, and battery
Turbidity sensor (OBS)	- Optical backscatter sensor (ISO 7027, 880 nm) - Accuracy ±1–3% over 0–1000 NTU - Equipped with wiper
GPS module	- 66-channel GPS for real-time location tracking
Data transmission	- Iridium satellite - Data stored in CSV format including observation time, buoy ID, coordinates, turbidity (NTU), and water temperature

Table 2
Specifications of the UAV.

Component	Specification
Model	Matrice 600 Pro
Weight	9.5 kg
Hovering accuracy	Vertical: ±0.5 m, Horizontal: ±1.5 m
Maximum wind resistance	8 m/s
Maximum flight speed	65 km/h
Hovering time	Payload 0 kg: 32 min, Payload 5.5 kg: 18 min

2.4 Data analysis and two-dimensional visualization

The workflow for data analysis and 2D visualization is illustrated in Fig. 2. This workflow integrates field measurements, UAV imagery, and computational analysis to generate high-resolution *SSC* maps. The process consists of three main components:

- OBS Sensor Calibration: *In situ* water samples were collected immediately after buoy deployment to convert turbidity (NTU) into *SSC* (mg/L).[13] Laboratory analysis and linear regression between OBS turbidity values and *SSC* provided a conversion formula for accurate *SSC* estimation.[14]
- Image Analysis and Pixel Intensity Extraction: UAV images were segmented into individual frames and decomposed into RGB bands. Since suspended inorganic sediments exhibit maximum reflectance in the red and NIR regions, the R-band pixel intensity, which is sensitive to *SSC* variations, was used for analysis.[15–17] Basic image preprocessing, including median filtering, was applied to minimize noise. Pixel intensity values were then extracted and normalized relative to a reference to compute the pixel intensity ratio (*PIR*).[18,19]
- 2D *SSC* Visualization: A conversion formula ($SSC = A \times PIR + B$) was obtained by correlating the *SSC* measured at buoy locations with the *PIR* extracted from UAV images.[20] This formula was applied to all pixels within the study area, generating a 2D map of *SSC*.

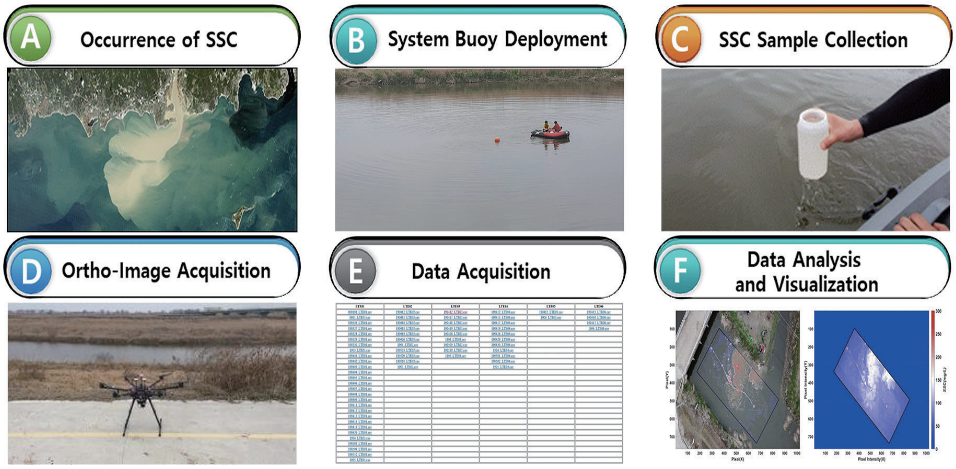

Fig. 2. (Color online) Workflow for data analysis and two-dimensional visualization..

3. Results and Discussion

3.1 Study area and data acquisition

The field implementation and verification of the system were conducted in a tributary of the Mangyeong River. This location was ideal owing to distinct *SSC* changes at the confluence and allowed strategic placement of observation buoys for spatial monitoring (Fig. 3). Four system buoys were deployed, and the UAV acquired orthomosaic imagery through a 10 min hovering flight.

3.2 Correlation between turbidity (NTU) and *SSC*

Prior to UAV orthomosaic acquisition, calibration using *in situ* water samples was performed to convert OBS turbidity (NTU) into *SSC* (mg/L). Figure 4 illustrates the correlation between the turbidity measured at each buoy and the laboratory *SSC* values.

The coefficient of determination (R^2) for individual buoys ranged from 0.80 to 0.86, indicating strong consistency. However, the integrated regression equation for all buoys yielded a lower R^2 of 0.68, likely owing to spatial heterogeneity in sediment properties (e.g., particle size, composition) across the study area.

Using the regression equation, we converted the OBS turbidity measurements into *SSC* time series for each buoy. The resulting *SSC* values ranged from 67.6 to 195.8 mg/L, with mean concentrations between 81.3 and 112.9 mg/L. The *SSC* time series generally converged toward the mean values, indicating a relatively stable average sediment load during the observation period. Table 3 summarizes the statistical characteristics of *SSC* at each buoy, including minimum, maximum, mean, and standard deviation values.

Fig. 3. (Color online) Field-selected study site.

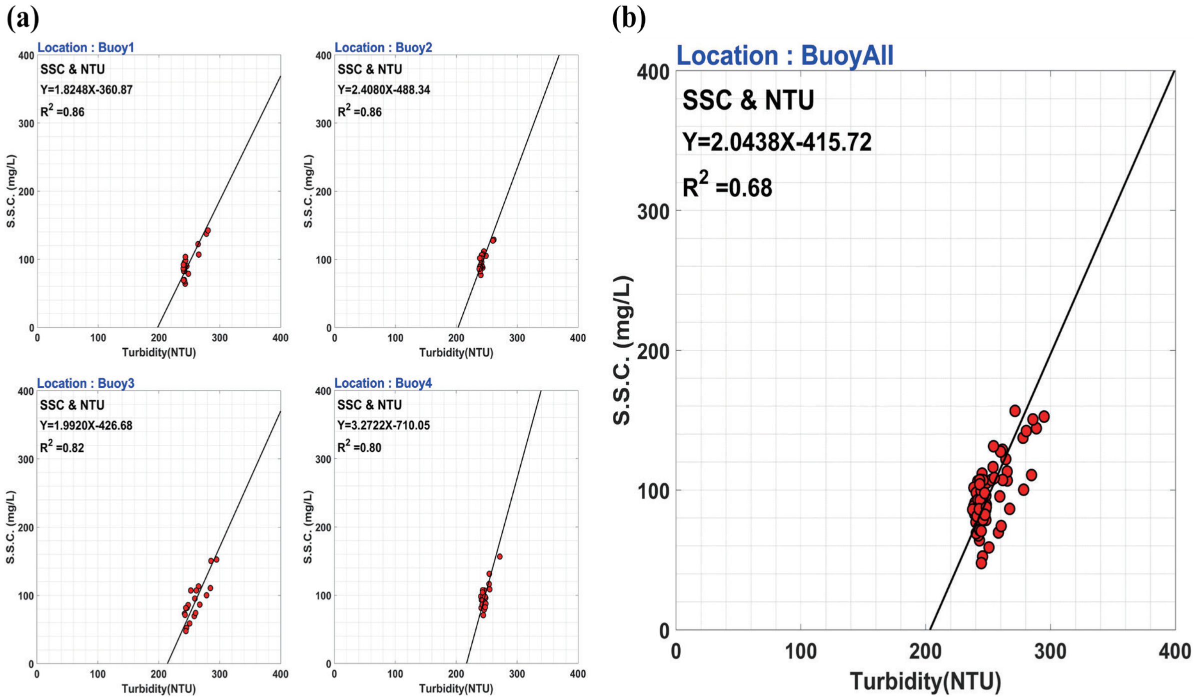

Fig. 4. (Color online) Correlation between OBS turbidity (NTU) and SSC (mg/L): (a) individual buoy analysis and (b) integrated data analysis.

Table 3
Statistical analysis results of suspended sediment concentrations of integrated data analysis.

	Buoy1	Buoy2	Buoy3	Buoy4
Min *SSC*	69.3	37.6	76.2	75.2
Max *SSC*	163.9	133.8	195.8	139.2
Mean *SSC*	91.4	81.3	112.9	91.3
Standard deviation	25.7	13.7	33.2	14.0

The *SSC* time series also revealed that most values fluctuated around the mean, with occasional peaks reflecting episodic sediment transport events. Figure 5 presents the temporal *SSC* variations for all four buoys, highlighting both the consistency of average sediment loads and the localized variability across the observation area.

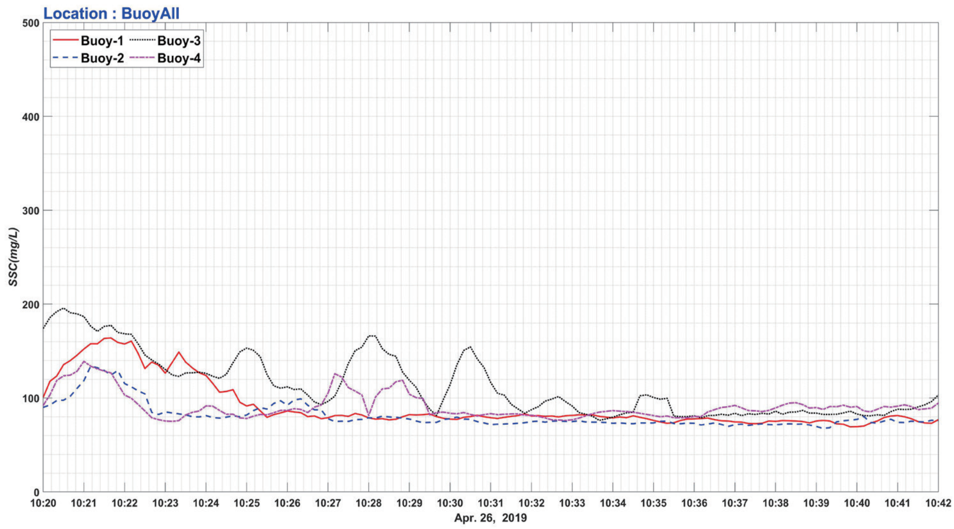

Fig. 5. (Color online) Time series of *SSC* (mg/L) at each buoy derived from OBS measurements using the regression equation.

3.3 Correlation between *PIR* and *SSC*

As previously described in Sect. 2.4, the linear relationship between *PIR* and *SSC* was established through calibration using UAV imagery and *in situ* measurements. In this section, the correlation is quantitatively evaluated on the basis of field data. As shown in Fig. 6, *PIR* and *SSC* exhibited a strong positive linear relationship, with a coefficient of determination of R^2 = 0.84.

This result demonstrates that the optical characteristics (*PIR*) of the UAV image can be used to quantitatively estimate surface *SSC*. The resulting regression equation ($SSC = 2.4282 \times PIR - 48.60$) was applied for *SSC* estimation. This specific linear relationship is a site-specific result reflecting the characteristics of suspended matter at the Mangyeong River confluence point during the observation period; thus, recalibration through field measurement is necessary for application to other water bodies or seasonal conditions.

3.4 Spatiotemporal variation of 2D *SSC*

Figure 7 shows the two-dimensional distribution of surface *SSC*, generated at 60 s intervals using the final conversion formula.

At the initial stage (T + 0 s), a high *SSC* region (>190 mg/L) was observed near the tributary confluence. As time progressed, the sediment plume dispersed along the main channel, and the high-concentration zone gradually diminished, disappearing after approximately 300 s. For a more detailed examination, *SSC* time series were extracted from six arbitrarily selected points (P1–P6) (see Fig. 8).

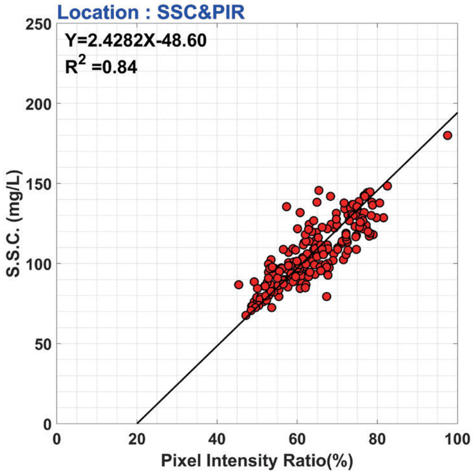

Fig. 6. (Color online) Correlation between *PIR* from UAV imagery and *SSC* (mg/L).

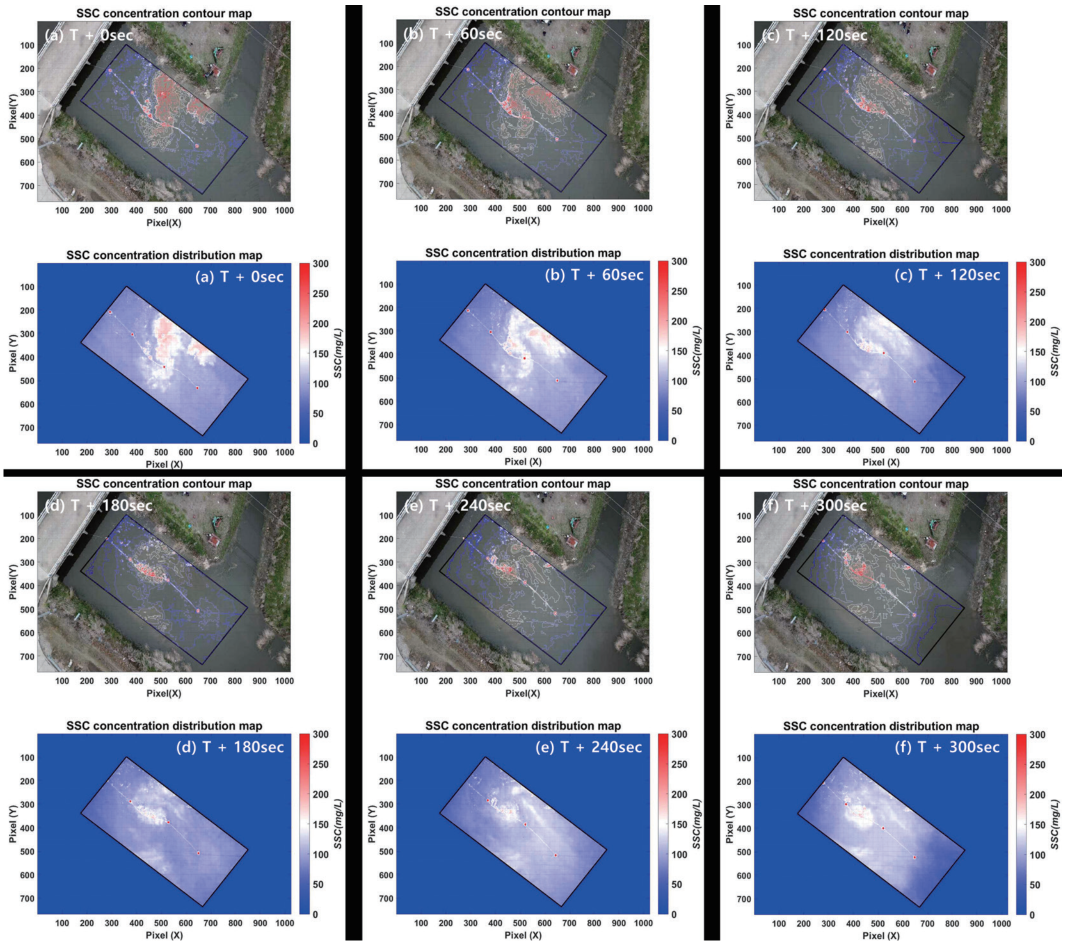

Fig. 7. (Color online) Temporal variation in 2D *SSC* distribution (T + 0 s to T + 300 s).

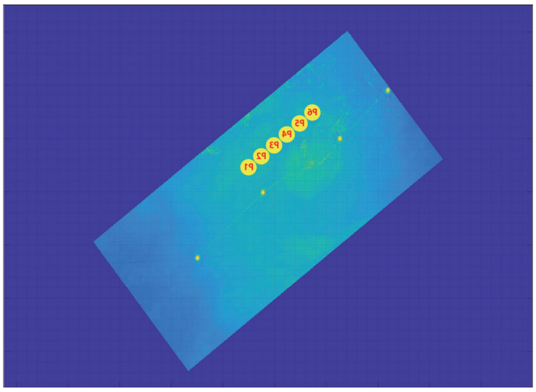

Fig. 8. (Color online) Time series of *SSC* variation at selected points P1–P6.

Table 4
Statistical analysis results of *SSC* at P1–P6.

	P1	P2	P3	P4	P5	P6
Min SSC	96.2	90.2	105.4	105.2	87.1	91.7
Max SSC	155.0	176.1	192.7	153.5	126.4	132.4
Mean SSC	122.0	124.5	128.5	125.0	112.6	108.0
Standard Deviation	13.7	17.1	17.6	11.3	9.8	9.8

The results indicate that the points closer to the source (P1–P4) showed higher maximum concentrations. This demonstrates that the developed system can visually and quantitatively track the entire process of suspended sediment generation, movement, diffusion, and dilution, providing information that is impossible to obtain with conventional point-based sensors alone.

A key limitation of this approach is that, because it relies on optical signals, monitoring is effectively restricted to the surface layer (i.e., the optically accessible upper water column).[21,22] Vertical *SSC* structures such as near-bed resuspension layers, mid-depth intrusions, and stratification-induced particle trapping are not directly observed, and apparent surface homogeneity may mask actual gradients with depth.[23,24] In environments with strong vertical shear, density stratification, or wave–current interactions, the surface *SSC* may diverge from the depth-integrated (volumetric) *SSC*.[24] Therefore, interpretations of plume area, dilution rates, and mass balance should be approached conservatively.[25] Furthermore, in highly turbid waters or waters affected by colored dissolved organic matter (CDOM) or algal pigments, the *PIR–SSC* relationship can become nonlinear or saturated,[26] making careful and site-specific calibration essential.[27]

4. Conclusions

In this study, we developed and field-validated a monitoring system that integrates real-time buoy observations with UAV imagery to retrieve high-resolution spatiotemporal distributions of surface *SSC*. By combining turbidity (NTU), water temperature, and position data transmitted from buoys with UAV orthomosaics, the system simultaneously captured temporal evolution and spatial dispersion of sediment plumes in a natural river setting. Field results confirmed a strong correlation between OBS turbidity and laboratorymeasured *SSC*, and a strong linear relationship between *PIR* and *SSC* (R^2 = 0.84), indicating that, with appropriate standardization and coregistration, UAV imagery alone can support the quantitative estimation of surface *SSC*.

Applying the final conversion equation yielded two-dimensional surface *SSC* maps that clearly depict sediment generation, transport, diffusion, and dilution. These products support practical tasks such as plume boundary delineation, hotspot identification, and short-timescale variability assessment, and they provide valuable reference data for the calibration/validation of numerical models and for the development of remote-sensing algorithms. In addition, linking with existing infrastructure (e.g., site CCTV) can reduce gaps between UAV flights and enable quasi-real-time surveillance, improving operational flexibility, scalability, and cost efficiency.

Future work should prioritize three directions. First, assimilate limited vertical profiles (e.g., ADCP/OBS casts, pump sampling) into threedimensional hydrosedimentary models to infer volumetric *SSC* from surface maps. Second, introduce NIR, multispectral/hyperspectral, and polarization channels and standardize *in situ* radiometric, atmospheric, and surface (glint/tilt) corrections to enhance predictive stability and transferability across optical and hydraulic conditions. Third, extend applications to estuaries and coastal zones and to high-turbidity flood periods or reservoir draw-down conditions; in parallel, establish automated quality control and standard operating procedures and integrate with persistent surveillance (e.g., CCTV) to strengthen quasirealtime operations.

Acknowledgments

This work was supported by Korea Environment Industry & Technology Institute (KEITI) through Climate Resilient R&D Project for Water-Related Disaster Management, funded by Korea Ministry of Climate, Energy, Environment (MCEE)(RS-2024-00335526).

References

1 G. S. Bilotta and R. E. Brazier: Water Res. **42** (2008) 2849. https://doi.org/10.1016/j.watres.2008.03.018
2 K. A. Dafforn, T. M. Glasby, L. Airoldi, N. K. Rivero, M. Mayer-Pinto, and E. L. Johnston: Front. Ecol. Environ. **13** (2015) 82. https://doi.org/10.1890/140050
3 T. M. Wood and C. D. Smith: Light attenuation and erosion characteristics of fine sediments in a highly turbid, shallow, Great Basin Lake—Malheur Lake, Oregon, 2017–18 (U.S. Geological Survey, 2022) Scientific Investigations Report 2022–5056. https://doi.org/10.3133/sir20225056
4 P. J. Wood and P. D. Armitage: Environ. Manage. **21** (1997) 203.
5 L. A. Levin, W. Ekau, A. J. Gooday, F. Jorissen, J. J. Middelburg, S. W. A. Naqvi, C. Neira, N. N. Rabalais, and J. Zhang: Biogeosciences **6** (2009) 2063. https://doi.org/10.5194/bg-6-2063-2009
6 S. Cho: The Asia Business Daily. https://cm.asiae.co.kr/en/article/2021040910062779046 (accessed July 2026).
7 T. K. Edwards and G. D. Glysson: Field methods for measurement of fluvial sediment (U.S. Geological Survey, Reston, Virginia, 1988) Open-File Report 86–531.
8 R. Cassidy and P. Jordan: J. Hydrol. **405** (2011) 182. https://doi.org/10.1016/j.jhydrol.2011.05.020
9 R. O. Strobl and P. D. Robillard: J. Environ. Manage. **87** (2008) 639. https://doi.org/10.1016/j.jenvman.2007.03.001
10 J. Droujko and P. Molnar: Sci. Rep. **12** (2022) 10341. https://doi.org/10.1038/s41598-022-14228-4

11 Y. Wang, S. Li, Y. Lin, and M. Wang: Sensors **21** (2021) 7397. https://doi.org/10.3390/s21217397
12 DJI: Matrice 600 Pro User Manual (DJI, Shenzhen, 2018). https://www.dji.com/downloads/products/matrice600-pro
13 Coastal Wiki: Optical backscatter point sensor (OBS). https://www.coastalwiki.org/wiki/Optical_backscatter_point_sensor_%28OBS%29 (accessed July 2026).
14 National Institute of Fisheries Science: Marine environment test methods (Ministry of Oceans and Fisheries, 2023) Notification No. 2023-5. https://www.nifs.go.kr/board/actionBoard0052List.do?selectPage=4&&BBS_CL_CD=A
15 R. P. Bukata, J. H. Jerome, A. S. Kondratyev, and D. V. Pozdnyakov: Optical Properties and Remote Sensing of Inland and Coastal Waters (CRC Press, 2018).
16 Reisinger, J. C. Gibeaut, and P. E. Tissot: Front. Mar. Sci. **4** (2017) 233. https://doi.org/10.3389/fmars.2017.00233
17 T. M. Pavelsky and L. C. Smith: Water Resour. Res. **45** (2009). https://doi.org/10.1029/2008WR007424
18 G. R. Arce: Nonlinear Signal Processing: A Statistical Approach (John Wiley & Sons, 2004).
19 Hernández-Cruz, M. Vásquez-Ortiz, C. Canet, and J. Prado-Molina: Appl. Ecol. Environ. Res. **17** (2019) 6549. https://doi.org/10.15666/aeer/1703_65496562
20 H. Noh, S. Kwon, Y. S. Park, and S. B. Woo: Appl. Ocean Res. **145** (2024) 103940. https://doi.org/10.1016/j.apor.2024.103940
21 E. Boss, C. R. Sherwood, P. Hill, and T. Milligan: Appl. Sci. **8** (2018) 2692. https://doi.org/10.3390/app8122692
22 J. Downing: Cont. Shelf Res. **26** (2006) 2299. https://doi.org/10.1016/j.csr.2006.07.018
23 J. Moodie, J. A. Nittrouer, H. Ma, B. N. Carlson, Y. Wang, M. P. Lamb, and G. Parker: Water Resour. Res. **58** (2022) e2020WR027192. https://doi.org/10.1029/2020WR027192
24 M. Liu, D. Chen, H. G. Sun, and F. Zhang: Fractal Fract. **7** (2023) 456. https://doi.org/10.3390/fractalfract7060456
25 P. N. Owens, R. J. Batalla, A. J. Collins, B. Gomez, D. M. Hicks, A. J. Horowitz, G. M. Kondolf, M. Marden, M. J. Page, D. H. Peacock, E. L. Petticrew, W. Salomons, and N. A. Trustrum: River Res. Appl. **21** (2005) 693. https://doi.org/10.1002/rra.878
26 W. Zhu, Q. Yu, Y. Q. Tian, B. L. Becker, T. Zheng, and H. J. Carrick: Remote Sens. Environ. **140** (2014) 766. https://doi.org/10.1016/j.rse.2013.10.015
27 Y. Lu, J. Chen, Z. Han, Q. Xu, M. Peart, C. N. Ng, F. Y. S. Lee, B. C. H. Hau, and W. W. Y. Law: Sci. Total Environ. **947** (2024) 174483. https://doi.org/10.1016/j.scitotenv.2024.174483

About the Authors

Hyung-Suk Kim received his Ph.D. degree in civil engineering from Hokkaido University, Japan. He served as a junior and senior researcher at the Korea Institute of Civil Engineering and Building Technology (KICT). Since 2020, he has been an assistant professor in the Department of Civil Engineering at Kunsan National University, Republic of Korea. His research interests include hydraulics and coastal engineering, sediment transport and morphodynamics, scouring, and ecological modeling of fish populations. (hskim0824@kunsan.ac.kr)

Gyu-Seok Han is currently pursuing his Ph.D. degree in the Department of Civil Engineering at Kunsan National University, Republic of Korea. His research interests include coastal and hydraulic engineering, sediment transport and erosion/deposition analysis, sediment grain size analysis, physical oceanography, marine environmental monitoring, and overall data analysis and field surveys in the aquatic environment sector.
(hgs712@hanmail.net)

Jae-Seon Yoon received his Ph.D. degree in civil engineering from Hanyang University, majoring in water resources and coastal engineering. He is currently conducting various numerical and hydraulic model studies at the Rural Research Institute of the Korea Rural Community Corporation. (jsun0757@ekr.or.kr)

Woochul Kang received his Ph.D. degree from Colorado State University, USA, in 2019. From 2019 to 2024, he was a researcher at the Korea Institute of Civil Engineering and Building Technology (KICT). He is currently an assistant professor at Kongju National University. While his research interests cover a wide range of fields, his main area involves integrating water engineering—his primary major—with various technologies such as remote sensing and AI. (kang@kongju.ac.kr)

Seung-Bae Choi is currently pursuing his Ph.D. degree in the Department of Civil Engineering at Kunsan National University, Republic of Korea. His research interests include coastal engineering, sediment transport, physical oceanography, environmental monitoring, and data analysis for coastal engineering. (ace8978@kunsan.ac.kr)